HHS Public Access

Author manuscript

J Cell Physiol. Author manuscript; available in PMC 2019 September 03.

Published in final edited form as:

J Cell Physiol. 2019 August ; 234(10): 18602–18614. doi:10.1002/jcp.28498.

Hydrogen sulfide attenuates homocysteine-induced osteoblast dysfunction by inhibiting mitochondrial toxicity

Yuankun Zhai, **Jyotirmaya Behera**, **Suresh C. Tyagi**, **Neetu Tyagi**

Department of Physiology, School of Medicine, University of Louisville, Louisville, Kentucky

Abstract

Homocysteine (Hcy) is detrimental to bone health in a mouse model of diet-induced hyperhomocysteinemia (HHcy). However, little is known about Hcy-mediated osteoblast dysfunction via mitochondrial oxidative damage. Hydrogen sulfide (H_2S) has potent antioxidant, anti-inflammatory, and antiapoptotic effects. In this study, we hypothesized that the H_2S mediated recovery of osteoblast dysfunction by maintaining mitochondrial biogenesis in Hcy-treated osteoblast cultures in vitro. MC3T3-E1 osteoblastic cells were exposed to Hcy treatment in the presence or absence of an H_2S donor (NaHS). Cell viability, osteogenic differentiation, reactive oxygen species (ROS) production were determined. Mitochondrial DNA copy number, adenosine triphosphate (ATP) production, and oxygen consumption were also measured. Our results demonstrated that administration of Hcy increases the intracellular Hcy level and decreases intracellular H_2S level and expression of the cystathionine β-synthase/Cystathionine γ-lyase system, thereby inhibiting osteogenic differentiation. Pretreatment with NaHS attenuated Hcy-induced mitochondrial toxicity (production of total ROS and mito-ROS, ratio of mitochondrial fission (DRP-1)/fusion (Mfn-2)) and restored ATP production and mitochondrial DNA copy numbers as well as oxygen consumption in the osteoblast as compared with the control, indicating its protective effects against Hcy-induced mitochondrial toxicity. In addition, NaHS also decreased the release of cytochrome *c* from the mitochondria to the cytosol, which induces cell apoptosis. Finally, flow cytometry confirmed that NaHS can rescue cells from apoptosis induced by Hcy. Our studies strongly suggest that NaHS has beneficial effects on mitochondrial toxicity, and could be developed as a potential therapeutic agent against HHcy-induced mitochondrial dysfunction in cultured osteoblasts in vitro.

Keywords

hydrogen sulfide; methionine; mitochondria; osteoblast; oxidative stress

Correspondence: Neetu Tyagi, Department of Physiology, Health Sciences Center, A-1201, University of Louisville, Louisville, KY 40202. n0tyag01@louisville.edu.

AUTHOR CONTRIBUTIONS

Y. Z. and J. B. carried out the experiment and analyzed the data. Y. Z. wrote the manuscript with support from J. B. and N. T., and S. C. T. and N. T. helped supervise this project. All authors discussed the results and contributed to the final manuscript.

CONFLICT OF INTERESTS

The authors declare that there are no conflict of interests.

1 | INTRODUCTION

Homocysteine (Hcy) is a nonessential, sulfur-containing, nonproteinogenic amino acid synthesized during methionine metabolism. However, B-group vitamins play an important role in homocysteine turnover, either being recycled back into methionine or converted into cysteine (Skovierova et al., 2016). Hcy is formed in almost all the tissues, but blood plasma Hcy concentrations highly depend on appropriate intracellular Hcy metabolism in the various organs such as the liver and kidneys (Behera, Bala, Nuru, Tyagi, & Tyagi, 2017). An imbalance in Hcy metabolism causes a higher concentration of Hcy, a condition typically called hyperhomocysteinemia (HHcy), and this will lead to cellular toxicity through homocysteine auto-oxidation and reactive oxygen species (ROS) generation. This leads to the conglomeration of pathological diseases, such as neurological disorders, chronic kidney disease, gastrointestinal disorders, cancer, and the development of congenital defects (Skovierova et al., 2016). Recent research has demonstrated that increased plasma Hcy has been linked to the increased incidence of bone loss and osteoporosis-related fracture. One of these clinical trials reported that plasma Hcy level in elderly patients with osteoporosis is higher than that of nonosteoporotic patients (Zhu, Shen, Cheng, Fan, & Lin, 2016), and can even be a pathological biomarker for bone disease (Behera et al., 2017).

Mitochondria are a major source of adenosine triphosphate (ATP), which they make by oxidative phosphorylation, and they also produce ROS (Kato et al., 2017). Recent reports suggest that mitochondria deteriorate with age, losing respiratory activity, accumulating damage to their DNA (mitochondrial DNA [mtDNA]), and producing excessive amounts of ROS (Lane, Hilsabeck, & Rea, 2015). Current evidence suggests that mitochondrial dysfunction is a key factor contributing to aging and age-related diseases, such as cancer, intestinal barrier dysfunction, depression, chronic obstructive pulmonary disease, diabetes, and bone disease (Kato et al., 2017). Osteoporosis is one such bone disease, which is characterized by low bone mass, deteriorated bone structure, and increased bone fractures. Osteoblasts, which are responsible for the synthesis and mineralization of bone during both initial bone formation and later bone remodeling, were observed to exhibit robust mitochondrial biogenesis, increased ATP production, and decreased mitochondrial stress. Oxidative stress on mitochondria can impair their function via opening of the mitochondrial permeability transition pore, which are regulated by cyclophilin D (CypD) that disrupts mitochondrial membrane integrity, and CypD deletion protects against mitochondria impairment to prevent aging bone loss (Shum et al., 2016). Inhibition of mitochondrial activity or an increase in mitochondrial superoxide production significantly suppressed osteoblast differentiation (Gao et al., 2018). As homocysteine is detrimental to bone health, the mechanistic basis of homocysteine mediated mitochondrial dysfunction and subsequent inhibition osteoblast function has not been fully elucidated yet.

Hydrogen sulfide (H_2S) is an easily recognizable colorless gas with characterized by a peculiar smell of rotten eggs (Y. Zhai, Tyagi, & Tyagi, 2017). It has been known as a novel gasotransmitter, and it mediates multiple physiological functions, not only providing anti-inflammatory, antioxidative and antiapoptotic effects, but also having a positive effect on skeletal and bone development. So the osteoprotective effects of H_2S have piqued many researchers' attention in recent years (Y. Zhai, Tyagi, et al., 2017). The recent study reported

that administration of sodium hydrogen sulfide (NaHS) protects from H_2O_2-induced oxidative damage and osteoblast dysfunction in murine preosteoblast cell lines. (Xu et al., 2011). Another study has also demonstrated that NaHS prevents high glucose-induced damage to osteoblasts function through regulation of K^+-ATP channels (Liu et al., 2017). Additionally, NaHS inhibits dexamethasone-induced osteoblast damage through the activation of AMPK signaling (Yang et al., 2014). Other studies also reported that H_2S can alleviate the Hcy-induced toxicity in myocardial injury (Chang et al., 2008), neuronal death (Liu et al., 2017), hypertension (Sen, Mishra, Tyagi, & Tyagi, 2010), cognitive dysfunction (M. Li et al., 2017) and kidney injury (Kasinath, 2014).

However, the protective role of H_2S in Hcy-induced osteoblast dysfunction by regulating mitochondrial stress is not well studied. In the present study, we addressed the potential role of H_2S against Hcy-induced decreased bone mineralization in vitro. We demonstrate that Hcy enhances oxidative stress and further enhances the mitochondrial toxicity and ROS generation through the attenuation of antioxidant systems in the osteoblast. Treatment with H_2S can promote normal osteoblast mineralization and restoration of mitochondrial function, and thus displays an osteoprotective property.

2 | MATERIALS AND METHODS

2.1 | Chemicals and reagents

DL-Homocysteine, NaHS, and thiazolyl blue tetrazolium bromide (MTT) were purchased from Sigma-Aldrich (St. Louis, MO). TRIzol for RNA isolation was obtained from Thermo Fisher Scientific (Waltham, MA). Primary antibodies against heme oxygenase-1 (HO-1), *S*-adenosylhomocysteine, superoxide dismutase 2 (SOD-2), catalase-1, NADPH oxidase 2 (NOX2)/4, OPG, RANKL, β-catenin, BMP-2, Runx-2, Osterix and horseradish peroxidase (HRP)-conjugated antibodies were supplied from Santa Cruz Biotechnology (Dallas, TX). Primary antibodies against osteocalcin, osteopontin and glyceraldehyde 3-phosphate dehydrogenase (GAPDH) were obtained from Millipore (Darmstadt, Germany). Oxygen consumption rate kit was purchased from Abcam (Cambridge, MA). 4′,6-Diamidino-2-phenylindole and 2′,7′-dichlorodihydrofluorescein diacetate (H2DCFDA) were obtained from Invitrogen (Carlsbad, CA). Alpha minimum essential medium (*α*-MEM) culture media was purchased from Gibco (Grand Island, NY). Penicillin and streptomycin were purchased from American Type Culture Collection (ATCC, Manassas, VA).

2.2 | Cell culture and treatment

Murine preosteoblast MC3T3-E1 subclone 4 (ATCC; CRL-2593™) derived from C57BL/6 mouse was purchased from the American Type Culture Collection (ATCC). Cells were seeded at 1×10^5 cells/ml into 75 cm^2 flasks and maintained in *α*-MEM supplemented with 10% fetal bovine serum and antibiotics (1% penicillin/streptomycin plus 2.5 mg/L amphotericin B), incubated at 37°C in 5% humidified CO_2 atmosphere, the basic medium was changed every 3 days until up to 90% confluence. Then, the cells were trypsinized and seeded onto six-well plate and given treatment.

2.2.1 | Treatment groups—Murine preosteoblast MC3T3-E1 cells were used for in vitro study and given the following treatments: (a) Control (no treatment), (b) Hcy (various concentrations: 50, 100, and 300 μM), (c) Hcy + NaHS (300 μM + 30 μM), (d) NaHS (30 μM). Cells were given treatment for 24 hr and harvested for further experiments. The concentration of NaHS in this study was set to 30 μM, as described in our previous research (Behera, George, Voor, Tyagi, & Tyagi, 2018). To check the rescue effects of NaHS during the Hcy-induced osteoblast dysfunction, the concentration of Hcy and NaHS were set to 300 and 30 μM, respectively.

2.3 | Homocysteine measurement assay

This assay was used to measure the total homocysteine content in the experimental mouse plasma using a homocysteine assay kit from Crystal Chem, as per the manufacturer's instructions (Kriebitzsch et al., 2011).

2.4 | H_2S measurement assay

H_2S assay was followed as described in Kundu, Pushpakumar, Khundmiri, and Sen (2014). After treatment, cells were homogenized with fresh, cold PBS. Then, the homogenates were centrifuged, and the supernatants were collected (100 μl) and mixed with 350 μl PBS (7.4) and 250 μl 1% zinc acetate in a microcentrifuge tube. Then *N,N*-dimethyl-*p*-phenylenediamine sulfate (prepared with 7.2 M HCl, 20 mM, 133 μl) and $FeCl_3$ solutions (prepared with 1.2 M HCl, 30 mM, 133 μl) were added into the mixture. The tubes were sealed with parafilm and incubated at 37°C for 45 min. Then, the reaction was stopped by the addition of trichloroacetic acid solution (10%, w/v, 250 μl), followed by centrifugation (12 000 rpm, 5 min). The samples and standards were transferred into a 96-well plate, and the absorbance was measured at 670 nm in a spectrophotometer. The calibration curve for H_2S was obtained using known concentrations of NaHS (0 to 200 μmol/L).

2.5 | Cell viability assay by MTT method

Cell viability was evaluated by using the MTT method as previously described (Behera et al., 2018). Briefly, MC3T3-E1 cells were seeded at 5×10^3 cells per well in a 96-well plate and allowed to proliferate under different treatment conditions. After treatment, the cells were incubated with MTT (0.5 mg/ml) for 4 hr at 37°C. After formation of formazan crystals, the culture medium containing MTT was removed and replaced with 150 μl of DMSO. Absorbance at 570 nm was measured using a spectrophotometric plate reader (BioTek, Winooski, VT). Cell viability was determined by a ratio of average absorbance in treatment cells to the average absorbance in control cells, and normalized with the control group.

2.6 | Intracellular ROS and mitochondria-ROS imaging by fluorescence microscopy

Intracellular ROS production was estimated by using 6-carboxy-2′, 7′-dichlorodihydrofluorescein diacetate (carboxy-H2DCFDA; Molecular Probes, Eugene, OR) staining, ROS production in mitochondria was stained by MitoSOX™ (Molecular Probes) and nuclei were stained by Hoechst 33342 (Molecular Probes). Briefly, cells were cultured in an eight-well chamber. Following treatments, cells were stained with the carboxy-

H2DCFDA fluorescence probe (25 μM, 100 μl/well) for total ROS staining, or MitoSOX green for mitochondria ROS detection, and incubated for 30 min at 37°C. Following incubation, cells were fixed with 4% paraformaldehyde for 10 min. Images were photographed under the laser scanning confocal microscope (Olympus FluoView1000).

2.7 | Mitochondria membrane potential (MMP) was detected by JC-1 intake

MMP was performed as previously described in Choi's method (Choi, 2011). A JC-1 intake assay kit (Cayman Chemical, Ann Arbor, MI) was used to demonstrate the changes in the MMP in cells. Cells were incubated with JC-1 for 20 min at 37°C, washed twice in PBS, and then fluorescence was measured using excitation/emission = 550/600 nm. The data was presented as a percentage of the value for the control.

2.8 | ATP detection assay

This assay was used to measure the ATP production in experimental samples using an ATP determination kit from Molecular Probes, as per the manufacturer's instructions.

2.9 | Oxygen consumption rate detection

This assay was used to measure the oxygen consumption rate in experimental samples using an oxygen consumption assay kit from Abcam, as per the manufacturer's instructions.

2.10 | Mitochondrial copy number

The mitochondrial copy number was measured as previously described by Sharma et al. (2013). The DNA primers used were designed to detect COX-1 as marker for mitochondrial DNA, and β-actin for nuclear DNA. Polymerase chain reaction (PCR) was used to amplify mtDNA and nuclear DNA (nDNA) products. Relative values of mitochondrial DNA products (COX-1) and nuclear DNA products (β-actin) within each sample were used to obtain a ratio of mtDNA to nDNA. The following primer sequences were used for reverse transcription polymerase chain reaction (RT-PCR): COX-1 (forward: 5′-ATTGCCCTCCCCTCTCTACGCA-3′, reverse: 5′-CGTAGCTTCAGTATCATTGGTGCCC-3′), and primer of β-actin (forward: 5′-CCATGTTCCAAAACCATTCC-3′, reverse: 5′-GGGCAACCTTCCCAATAAAT-3′).

2.11 | RT-PCR analysis

MC3T3-E1 cells were seeded in 60 cm^2 dishes (10^4 cells/cm^2) and treatment was given for triplicates. Cells were treated with either 300 μM homocysteine, 30 μM NaHS, or both of them. After being treated for 24 hr, RNA was harvested using the TRIzol Reagent (Gibco) according to the manufacturer's instructions. The concentration and purity of total RNA was measured by using the NanoDrop 1000 spectrophotometer (Thermo Fisher Scientific, Waltham, MA). RT-PCR was performed by using ImProm-II™ Reverse Transcription kit (Promega Corporation, Madison, WI). A reverse transcription program on the DNA Engine Peltier Thermal Cycler (Bio-Rad Laboratories, Hercules, CA) was used to make the complimentary DNA (cDNA) by using 2 μg of the RNA. The program consisted of a denaturing cycle at 70°C for 6 min and then a reverse transcription cycle at 25°C for 2 min, 42°C for 50 min, 75°C for 5 min. Then 2 μl of cDNA (incubated with gene primers and

nuclease-free water for a final volume of 20 μl) from each sample was used for a gene amplification cycle at 95°C for 7 min (95°C for 50 s, 55°C for 1 min, 72°C for 1 min) (× 34), 72°C for 5 min. Invitrogen synthesized the primers and the sequences are listed in Table 1. The amplified products were run on 1.5% agarose gel (using TAE buffer), and quantification was performed using Image Lab software (Bio-Rad Laboratories). The amplified products of the targeted genes were normalized with respective GAPDH as housekeeping control.

2.12 | Western blot analysis

Briefly, the cells were washed with ice-cold PBS after osteogenic induction, followed by treatments. Then cells were lysed in RIPA buffer (Invitrogen, Rockford, IL) supplemented with a protease inhibitor cocktail (Sigma-Aldrich, St. Louis, MO). Protein concentration was determined with Pierce Coomassie plus the Bradford assay (Thermo Fisher Scientific, Waltham, MA), and equal amounts of proteins (60 μg) were loaded on 8–15% separating gels based on the molecular weights of target proteins. Then proteins were transferred onto polyvinylidene difluoride (PVDF) membranes by electroblotting as described. PVDF membranes were incubated overnight with primary antibodies at 4°C. Then, the membranes were incubated with HRP conjugated anti-mouse or anti-rabbit secondary antibody (Santa Cruz Biotechnology, Dallas, TX) for 1 hr at room temperature, and protein bands were visualized with ECL Plus reagents (Cell Signaling Technology, Waltham, MA) and images were taken in ChemiDoc™ XRS + (Bio-Rad Laboratories, Hercules, CA). The intensity was qualified by Image Lab 5.2.1 software and the results were expressed as a ratio of target protein and housekeeping control GAPDH.

2.13 | ALP activity assay

ALP activity and staining were carried out to study the osteogenic potential of Murine preosteoblast MC3T3-E1 cells under experimental conditions, according to our previously published protocol (Behera et al., 2018) and others (Ming et al., 2013; Y. K. Zhai et al., 2014). Briefly, MC3T3-E1 cells were grown in an osteogenic medium in 12-well culture plates. After 9 days of osteogenic induction, the cells were fixed with 4% formaldehyde and stained with SIGMAFAST™ *p*-nitrophenyl phosphate tablets (catalog No. N1891; Sigma-Aldrich, St. Louis, MO), and the images were then photographed. The number, total area, and relative intensities of ALP-positive colonies were counted and analyzed by using the image analysis software Image-Pro® plus 6.0.

2.14 | In vitro mineralization/calcified nodules staining assay

Calcified nodules formed on the 14th day of culture were analyzed by Alizarin Red-S staining and quantification (Y. Zhai, Li, et al., 2017). The stained culture plates were photographed, and the areas and relative intensities of calcified nodules were quantified by using Image-Pro plus 6.0 software. Meanwhile, the staining was solubilized with 100 mM cetylpyridinium chloride (Sigma-Aldrich, St. Louis, MO) for 1 hr and measured using a spectrophotometer at 570 nm (Park, Seo, Kim, & Kang, 2012).

2.15 | Mitotracker green staining and imaging by fluorescence microscopy

Mitotracker green (Thermo Fisher Scientific, Waltham, MA) was used to stain the Mitochondria in cultured MC3T3-E1, according to the published protocol (S. Li & Yang, 2015). Briefly, MC3T3-E1 was treated with Hcy or NaHS for 24 hr. Then, MC3T3-E1 was labelled with 5 μM mitotracker green for 15 min at 37°C. Then, the cells were washed twice with sterile PBS and fixed with 4% paraformaldehyde for 12 min. After brief washing with sterile PBS, cells were observed under a scanning confocal microscope (Olympus FluoView1000, Shinjuku, Tokyo, Japan). Fluorescence intensity was quantified with Image J software (NIH, Bethesda, MD) and presented in % of relative fluorescence intensity.

2.16 | Annexin V/propidium iodide (PI) assay to determine cell apoptosis

The apoptosis of MC3T3-E1 cells following homocysteine or NaHS exposure was detected by annexin V-FITC detection assay kit (Sigma-Aldrich, St. Louis, MO) according to the manufacturer's instructions. Briefly, MC3T3-E1 cells were cultured and treated with either 300 μM homocysteine, 30 μM NaHS, or both of them. After being treated for 48 hr, cells were trypsinized, washed twice with PBS, and resuspended into single cells in 1X binding buffer. Then, cells were stained with annexin V-FITC (5 μl) and PI (10 μl) in 1X binding buffer and incubated for exactly 10 min at room temperature in the dark. The apoptosis of cells (positive staining) was detected with a BD Accuri™ C6 Plus Flow Cytometer and analyzed using the BD Accuri™ C6 Software (BD Biosciences, San Jose, CA).

2.17 | Statistical analyses

All the data in our examinations were derived from at least three replicates, with some detections having six or nine duplicates. Each experiment was repeated three times. All data were presented as mean ± standard deviation (*SD*) and analyzed using one-way analysis of variance followed by the least significant difference post hoc test by using SPSS 22.0 software (SPSS, Chicago, IL). The data were considered statistically significant at $p < 0.05$.

3 | RESULTS

3.1 | Effect of homocysteine on osteoblastic H_2S production and cell viability

To determine the detrimental effect of Hcy, MC3T3-E1 preosteoblasts were treated with different concentrations of Hcy for 24 hr. The data demonstrate that intracellular homocysteine levels were, indeed, increased in a dose-dependent manner, especially in the 100 and 300 μM groups when compared with the control group ($p < 0.01$; Figure 1a). Meanwhile, the H_2S production was also decreased significantly when compared with the untreated control condition. Furthermore, we evaluated the protein expression of cystathionine β-synthase (CBS) and cystathionine γ-lyase (CSE), which produce the H_2S, in the osteoblast cultures using protein western blot analysis. We found that both CBS and CSE were reduced significantly under treatment with the higher concentrations of homocysteine (Figure 1b,c). To check the effects on cell viability/proliferation, we performed both Hoechst 33342 staining and MTT method. The data revealed that less cell growth was observed in the higher Hcy concentration treated condition (Figure 1d). In addition, cell number was also, indeed, reduced under higher Hcy concentration (Figure 1e). MTT viability also revealed

that cell viability was significantly reduced under higher Hcy concentration (100 and 300 μM; Figure 1f).

3.2 | Effect of homocysteine on osteoblast mineralization and ROS production

To address the role of Hcy in preosteoblast-derived osteogenesis, MC3T3-E1 cells were cultured and differentiated in vitro under osteogenic induction medium for 14 days. Our data indicate that Hcy (100 and 300 μM) exhibited a decrease in ALP activity and staining on Day 9 in the osteogenic medium (Figure 2a,b) when compared with the control group. Alizarin red staining (ARS) was also performed to investigate whether the Hcy resulted in a decreased osteoblast mineralization in vitro. The data revealed that Hcy (dose-dependent manner) reduced the mineralized nodule formation on Day 14 after positive ARS staining (Figure 2c,d) compared with control. In addition, we also tested the Hcy-induced ROS generation in cultured osteoblast cells by using carboxy-H2DCFDA fluorescence staining. The data suggested that Hcy also enhances the ROS production in a dose-dependent manner, especially in the 300 μM homocysteine treatment condition in comparison to the control (Figure 2e).

3.3 | Effect of NaHS on Hcy-induced inhibition of H_2S production and osteoblast function

To evaluate the osteoprotective effect of NaHS on Hcy-altered H_2S production and osteoblast mineralization, we evaluated the metabolites of Hcy metabolism in parallel with osteoblast activity. We found that supplementation of NaHS reverses the Hcy-mediated ablation of H_2S production and elevation of intracellular Hcy when compared with the control (Figure 3a). Furthermore, expression of CBS and CSE also reversed under the administration of NaHS (Figure 3b,c). MTT assay also confirmed that NaHS reversed the Hcy-mediated loss of cell viability (Figure 3d).

We also tested the effect of NaHS on osteoblast proliferation. The data found that Hcy inhibits the osteoblast proliferation, inhibiting cell viability and lowering the total number of cells, but NaHS can reverse the Hcy-mediated effect (Figure 3d–f). Additionally, we observed the osteoprotective effect of NaHS on osteoblast mineralization. ARS staining in osteoblast culture confirmed that NaHS reverses the Hcy-mediated ablation of osteoblast differentiation and mineralization (Figure 3g,h). The data suggested that Hcy was detrimental to osteoblast differentiation by decreasing ALP activity in comparison to the control. However, administration of NaHS could reverse the Hcy-mediated effect (Figure 3i,j). We also evaluated the expression of osteogenic proteins, like osteopontin, COL3A1, Runx-2, and Osterix in osteoblast culture under osteogenic conditions. The data showed that NaHS reversed the Hcy-mediated reduction of osteogenic proteins (Figure 3k–m).

3.4 | Effect of NaHS on Hcy-induced ROS generation and suppression of antioxidant system in osteoblast

As we found that Hcy enhances the ROS generation in a dose-dependent manner in osteoblast culture (Figure 2e). Furthermore, we found that the administration of NaHS (H_2S donor) can reverse the ROS generation in osteoblast culture (Figure 4a). Earlier reports have suggested that NF-E2-related factor 2 (Nrf2) and Keap-1 are two important cytoprotective factors which exhibit antioxidant activity against oxidative injury, apoptosis, and

inflammatory effects (Loboda, Damulewicz, Pyza, Jozkowicz, & Dulak, 2016). Taking this into account, we also tested the expression of Nrf2 and Keap-1 in osteoblast culture under Hcy treatment with or without NaHS. The data revealed that Nrf2 expression was downregulated in Hcy ($p < 0.05$ vs. control). However, administration of NaHS reverses the Hcy-mediated effect (Figure 4b,c). Kelch like ECH associated protein 1 (Keap-1) level was, indeed, increased under Hcy treatment as compared with the control. However, NaHS reversed the Hcy-mediated reduction of Keap-1 expression in the Hcy + NaHS condition (Figure 4b,c).

Furthermore, HO-1, catalase, and SOD-1 enzyme expression was downregulated in the Hcy condition ($p < 0.01$ vs. control). However, the reduction in overall protein expression was reversed with the administration of NaHS (Figure 4d,e). RT-PCR analysis further confirmed that mRNA expression of these antioxidant systems (antioxidant transcription factor and enzymes) was found to be reversed under NaHS treatment in Hcy + NaHS condition (Figure 4f–h). However, Keap-1 mRNA expression remained increased under the Hcy condition (Figure 4f,g).

3.5 | Effect of NaHS on Hcy reduced mitochondrial biogenesis via induction of mitochondrial ROS production in osteoblast

Mitochondrial biogenesis is crucial for osteoblast differentiation, and it is always accompanied by increased ATP production and decreased mitochondrial oxidative stress. Inhibition of mitochondrial activity, or an increase in mitochondrial superoxide production, significantly suppressed osteoblast differentiation (Gao et al., 2018). Here, we showed that Hcy stimulates the mitochondrial ROS production in the osteoblast culture by using MitoSox Red staining along with confocal microscopy. NaHS treatment of the osteoblast culture can inhibit the generation of mitochondrial ROS (Figure 5a). Both ATP production and MMP were, indeed, reduced under Hcy treatment, but this change was reversed by the supplementation of NaHS (Figure 5b,c).

We also tested the mito-SOD-2 expression in isolated mitochondrial fractions of the osteoblast culture. The data found that mito-SOD-2 was lower in the Hcy group while NaHS can stimulate the expression of SOD-2, which can attenuate the superoxide in mitochondria (Figure 5d,e). Additionally, COX-1 expression was reduced under Hcy treatment in the culture condition (Figure 5f). Biogenesis of mitochondria is important for the differentiation of osteoblasts. We also performed mitochondrial biogenesis by studying mito-copy number under experimental conditions. We found that Hcy was detrimental to mito-copy numbers and showed that the mito-copy number was decreased. Administration of NaHS reverses the Hcy-mediated effect (Figure 5g).

Both mitochondrial fission and fusion are cellular processes required for mitochondrial homeostasis (Forni, Peloggia, Trudeau, Shirihai, & Kowaltowski, 2016). Drp-1, which controls mitochondrial fission, was increased under Hcy treatment in the osteoblast culture (Figure 5h,i). Similarly, mitofusin-2 (Mfn-2), which controls the fusion of mitochondria, was reduced significantly under the Hcy condition (Figure 5h,i). To further confirm the mitochondria dynamics, we stained mitochondria by using mitotracker green staining. The overall Hcy-mediated effect was, indeed, reversed by administration of NaHS in Hcy-treated

osteoblast culture. As we have shown in Figure 5h,i Hcy increases the expression of Drp-1 but inhibits the expression of Mfn-2. This means that Hcys increase the fission but decreases the fusion of mitochondria in the osteoblast, and these will induce the dysfunction of mitochondria, therefore decreasing the differentiation of osteoblasts. However, supplementation with NaHS can reverse these effects. Similarly, mitotracker green staining also showed that Hcy decreases the number of mitochondria, while NaHS can inhibit the decrease of mitochondrial numbers in the presence of excess Hcy (Figure 5k,l). Meanwhile, we also measured the change of oxygen consumption rate (OCR) within 120 min, as shown in Figure 5j. We found that OCR in Hcy group was decreased in comparison to the control group, while the OCR in Hcy + NaHS group was reversed in comparison to the Hcy condition. This data shows that NaHS is indispensable for mitochondrial biogenesis by balancing redox homeostasis and acts as an antioxidant system in osteoblasts.

3.6 | Effect of NaHS on Hcy-induced cell apoptosis in osteoblast

As we reported, Hcy can induce mitochondrial dysfunction by exaggerating mito-ROS in the osteoblasts (Figure 5a). Dysfunction of mitochondria always induces cell apoptosis. As we expected, Cytochrome *c* (Cyt C), which is released from mitochondria to cytosol and induces cell apoptosis, was increased in Hcy group ($p < 0.01$ vs. control). However, these effects were reversed by administration of NaHS (Figure 6a,b). Similarly, flow cytometry also showed the percentage of apoptosis increase in the Hcy group, but it was decreased in Hcy + NaHS group (Figure 6c,d). Taken together, these data conclude that NaHS has osteoprotective effects in the osteoblast culture by inhibiting Hcy-mediated mitochondrial apoptosis.

4 | DISCUSSION

Hcy-induced osteoblast dysfunction is known to contribute to the development of osteoporosis (Behera et al., 2018). The proposed molecular and cellular mechanism underlying the mitochondrial toxicity dependent pathological processes are not currently well understood. In the current study, to clarify the detailed mechanisms mitochondrial toxicity and mitochondria dependent apoptosis underlying the opposing effects of Hcy on the osteoblast, in vitro experiments were performed. We have reported here that Hcy treatment can induce a decrease in the osteoblast activity and bone formation in vitro, by activating apoptosis in comparison to the control. This noxious effect of Hcy was related to mitochondrial dysfunction. The signal transduction events associated with Hcy-induced mitochondrial dysfunction and inhibition of osteoblast activity are described in Figure 6c. Hcy-induced mitochondrial dysfunction mainly modulates apoptosis of the osteoblasts, and might be responsible for the initiation of mitochondrial ROS generation through decreased H_2S biosynthesis. Prolonged mitochondrial toxicity resulted in the decreased mitochondrial biogenesis, which could be involved in moderating the apoptosis of osteoblast.

Hcy is a sulfur-containing amino acid that functions as a key intermediate in methionine metabolism. However, there are studies which show a correlation between high levels of Hcy and a great number of pathological diseases, including cardiovascular disease, stroke, dementia, osteoporosis, macular degeneration, and certain types of cancer (Skovierova et al.,

2016). High plasma Hcy levels have been associated with an increased risk of fracture. Hcy induces apoptosis via the ROS-mediated mitochondrial pathway and nuclear factor-κB activation in human bone marrow stromal cells (hBMSCs), and contributes to the development of osteoporosis by reducing bone formation (Kim et al., 2006). Elevated homocysteine induced the apoptosis of bone marrow mesenchymal stem cells via ROS-induced activation of c-Jun N-terminal kinase signal, which provides more insight into the molecular mechanisms of hyperhomocysteinemia-related cardiovascular diseases (Cai et al., 2013). Hcy can also induce the dysfunction of osteoblasts, reducing bone formation by increasing oxidative stress (Kanazawa et al., 2017). However, Hcy-mediated mitochondrial toxicity dependent osteoblast dysfunction was not well studied. The present study showed that Hcy could upregulate the mitochondrial ROS generation in a dose-dependent manner, which led to mitochondrial toxicity, suggesting that the Hcy-induced upregulation of mitochondrial ROS could be the one of the pathological phenomena in cultured osteoblast in vitro (Figure 4). Additionally, in our study, with the accumulating mitochondrial ROS, the expression of mito-SOD-2 was decreased and other antioxidant enzyme systems such as HO-1 and catalase activity were downregulated. These conditions, however, were significantly improved by administration of NaHS (Figures 4 and 5).

On the basis of these observations, we suggested that excessive mitochondrial ROS production could increase the release of Cyt C, thereby resulting in osteoblast apoptosis (Figure 6). At present, there is a causal relationship between HHcy, macrophage dysfunction, and oxidative damage in animal models of genetic- and diet-induced HHcy (Behera et al., 2018; Zhang et al., 2015). However, the major proposed molecular and cellular mechanisms underlying the mito-toxicity and osteoblast dysfunction under Hcy are incompletely understood. Our findings provide direct evidence that mitochondrial dysfunction induced by Hcy treatment contributed to apoptotic osteoblast cell death, which might be the important mechanism by which Hcy reduces bone mineralization in vitro (Figures 3 and 6). Furthermore, Xi et al. (2016) have reported that Hcy-induced pyroptotic apoptosis in endothelial cells via caspase-1 inflammasome activation and mitochondrial dysfunction, which induced by the release of Cyt C from mitochondria to cytosol (Xi et al., 2016). In our study, Hcy treatment obviously increased the expression of Cyt C in cytosol, but decreased Cyt C expression in mitochondria, which indicated Cyt C release was increased by Hcy. Our study further showed that releasing of Cyt C was obviously suppressed and mitochondrial function was improved upon NaHS administration in osteoblast culture, suggesting that the release of Cyt C from mitochondria to cytosol could result from the mitochondrial toxicity in Hcy-treated osteoblasts (Figure 6a,b).

Homeostasis of functional mitochondria requires a balance between the rate of mitochondrial fusion and mitochondrial fission. The proteins that regulate mitochondrial dynamics are now associated with a broad range of cellular functions (Hollenbeck & Saxton, 2005). Mitochondrial fission and fusion are known to play important roles in maintaining the integrity of mitochondria and mitochondrial biogenesis. It can also be inferred from the results that increased fission events are associated with upregulation of DRP-1 expression under Hcy treatment (Figure 5). Similarly, mitochondrial fusion was found to be decreased by downregulation of Mfn-2 expression. In addition, when cells were treated with NaHS, these observed effects substantially improved. Moreover, the fission and fusion machinery

have been implicated in programmed cell death pathways (Okamoto & Shaw, 2005). Hcy has been shown to induce the apoptosis of endothelial cells, which has been reported in several studies (Tyagi, Ovechkin, Lominadze, Moshal, & Tyagi, 2006). We also found a significant increase in activation of apoptosis of cultured Hcy-treated cells, which was also normalized by NaHS treatment (Figure 6c,d).

Mitochondria transform carbohydrates and fatty acids into ATP, which can supply the power for the physiological activity of cellular events. Mitochondria usually deteriorate with age and oxidative damage, thereby losing respiratory and biogenesis activity (Lane et al., 2015). Dysfunction of mitochondria is the main reason for poor bone quality (Kato et al., 2017; Lane et al., 2015). Therefore, restoring the function of mitochondria could be a therapeutic target for bone loss. The work of Vacek et al. (2018), reported that Hcy was detrimental for normal mitochondrial ATP production in cultured vascular endothelium through a mitochondrial ROS dependent action. In accordance with earlier studies, we also presented in our study that Hcy significantly reduces the mitochondrial biogenesis by reducing the normal ATP synthesis, oxygen consumption rate, and mitochondrial copy number. However, administration of NaHS could reverse the Hcy-mediated detrimental effect on the mitochondrial function (Figure 5).

H_2S is a gas-signaling molecule that has multiple influences on physiological and pathological processes. Recent study found abnormal H_2S metabolism has been linked to defects in bone homeostasis in a mouse model of CBS-deficiency (Liu et al., 2014). In another study, estrogen deficiency causes decreased production of H_2S that leads to stimulation of osteoporotic bone loss in a mouse model of OVX-induced bone loss (Grassi et al., 2016). In our previous study, we also found that HHcy caused oxidative stress and altered bone formation by reducing the plasma level of H_2S in a high methionine diet-induced HHcy mice model (Behera et al., 2018). Therefore, H_2S is indispensable for bone homeostasis. In the current study, we hypothesized that Hcy also induced the dysfunction of mitochondria in osteoblasts by altering H_2S biosynthesis pathways in vitro, and NaHS administration could reverse the above phenotypes. The data revealed that NaHS administration could mitigate the Hcy-mediated reduction of CBS/CSE enzyme activity and H_2S production (Figure 3). Additionally, the data also reported that NaHS treatment could reverse the Hcy-mediated reduction of bone mineralization (Figure 3).

5 | CONCLUSION

It is inferred from the present study that Hcy causes oxidative damage and mitochondrial dysfunction. The present study also explored that observation comprehensively, and has provided the evidence of altered osteoblast differentiation and mineralization under high concentrations of Hcy. Together, we conclude that an excess of Hcy increases mitochondrial ROS production, causing an imbalance in mitochondrial biogenesis through fission/fusion, thereby also inhibiting cytochrome c release-mediated apoptosis and leading to cellular dysfunction. Treatment of NaHS restores these events (Figure 6).

ACKNOWLEDGMENT

The study was supported from National Institute of health (grant no. AR-067667).

Funding information

National Institute of health, Grant/Award Number: AR-067667

REFERENCES

Behera J, Bala J, Nuru M, Tyagi SC, & Tyagi N (2017). Homocysteine as a pathological biomarker for bone disease. Journal of Cellular Physiology, 232(10), 2704–2709. [PubMed: 27859269]

Behera J, George AK, Voor MJ, Tyagi SC, & Tyagi N (2018). Hydrogen sulfide epigenetically mitigates bone loss through OPG/RANKL regulation during hyperhomocysteinemia in mice. Bone, 114, 90–108. [PubMed: 29908298]

Cai B, Li X, Wang Y, Liu Y, Yang F, Chen H, … Lu Y (2013). Apoptosis of bone marrow mesenchymal stem cells caused by homocysteine via activating JNK signal. PLOS One, 8(5), e63561. [PubMed: 23667638]

Chang L, Geng B, Yu F, Zhao J, Jiang H, Du J, & Tang C (2008). Hydrogen sulfide inhibits myocardial injury induced by homocysteine in rats. Amino Acids, 34(4), 573–585. [PubMed: 18071843]

Choi EM (2011). Kaempferol protects MC3T3-E1 cells through antioxidant effect and regulation of mitochondrial function. Food and Chemical Toxicology, 49(8), 1800–1805. [PubMed: 21565246]

Forni MF, Peloggia J, Trudeau K, Shirihai O, & Kowaltowski AJ (2016). Murine mesenchymal stem cell commitment to differentiation is regulated by mitochondrial dynamics. Stem Cells, 34(3), 743–755. [PubMed: 26638184]

Gao J, Feng Z, Wang X, Zeng M, Liu J, Han S, … Liu J (2018). SIRT3/SOD2 maintains osteoblast differentiation and bone formation by regulating mitochondrial stress. Cell Death and Differentiation, 25(2), 229–240. [PubMed: 28914882]

Grassi F, Tyagi AM, Calvert JW, Gambari L, Walker LD, Yu M, … Pacifici R (2016). Hydrogen sulfide is a novel regulator of bone formation implicated in the bone loss induced by estrogen deficiency. Journal of Bone and Mineral Research, 31(5), 949–963. [PubMed: 26614970]

Hollenbeck PJ, & Saxton WM (2005). The axonal transport of mitochondria. Journal of Cell Science, 118(Pt 23), 5411–5419. [PubMed: 16306220]

Kanazawa I, Tomita T, Miyazaki S, Ozawa E, Yamamoto LA, & Sugimoto T (2017). Bazedoxifene ameliorates homocysteine-induced apoptosis and accumulation of advanced glycation end products by reducing oxidative stress in MC3T3-E1 cells. Calcified Tissue International, 100(3), 286–297. [PubMed: 27832315]

Kasinath BS (2014). Hydrogen sulfide to the rescue in obstructive kidney injury. Kidney International, 85(6), 1255–1258. [PubMed: 24875544]

Kato H, Han X, Yamaza H, Masuda K, Hirofuji Y, Sato H, … Nonaka K (2017). Direct effects of mitochondrial dysfunction on poor bone health in Leigh syndrome. Biochemical and Biophysical Research Communications, 493(1), 207–212. [PubMed: 28899781]

Kim DJ, Koh JM, Lee O, Kim NJ, Lee YS, Kim YS, … Kim GS (2006). Homocysteine enhances apoptosis in human bone marrow stromal cells. Bone, 39(3), 582–590. [PubMed: 16644300]

Kriebitzsch C, Verlinden L, Eelen G, van Schoor NM, Swart K, Lips P, … Verstuyf A (2011). 1,25-Dihydroxyvitamin D3 influences cellular homocysteine levels in murine preosteoblastic MC3T3-E1 cells by direct regulation of cystathionine beta-synthase. Journal of Bone and Mineral Research, 26(12), 2991–3000. [PubMed: 21898591]

Kundu S, Pushpakumar S, Khundmiri SJ, & Sen U (2014). Hydrogen sulfide mitigates hyperglycemic remodeling via liver kinase B1-adenosine monophosphate-activated protein kinase signaling. Biochi-mica et Biophysica Acta/General Subjects, 1843(12), 2816–2826.

Lane RK, Hilsabeck T, & Rea SL (2015). The role of mitochondrial dysfunction in age-related diseases. Biochimica et Biophysica Acta/General Subjects, 1847(11), 1387–1400.

Li M, Zhang P, Wei HJ, Li MH, Zou W, Li X, … Tang XQ (2017). Hydrogen sulfide ameliorates homocysteine-induced cognitive dysfunction by inhibition of reactive aldehydes involving upregulation of ALDH2. International Journal of Neuropsychopharmacology, 20(4), 305–315. [PubMed: 27988490]

Li S, & Yang G (2015). Hydrogen sulfide maintains mitochondrial DNA replication via demethylation of TFAM. Antioxidants & Redox Signaling, 23(7), 630–642. [PubMed: 25758951]

Liu Y, Liu J, Li X, Wang F, Xu X, & Wang C (2017). Exogenous H2S prevents high glucose-induced damage to osteoblasts through regulation of KATP channels. Biochimie, 137, 151–157. [PubMed: 28322929]

Liu Y, Yang R, Liu X, Zhou Y, Qu C, Kikuiri T, … Shi S (2014). Hydrogen sulfide maintains mesenchymal stem cell function and bone homeostasis via regulation of Ca(2 +) channel sulfhydration. Cell Stem Cell, 15(1), 66–78. [PubMed: 24726192]

Loboda A, Damulewicz M, Pyza E, Jozkowicz A, & Dulak J (2016). Role of Nrf2/HO-1 system in development, oxidative stress response and diseases: An evolutionarily conserved mechanism. Cellular and Molecular Life Science, 73(17), 3221–3247.

Ming LG, Lv X, Ma XN, Ge BF, Zhen P, Song P, … Chen KM (2013). The prenyl group contributes to activities of phytoestrogen 8-prenynaringenin in enhancing bone formation and inhibiting bone resorption in vitro. Endocrinology, 154(3), 1202–1214. [PubMed: 23389955]

Okamoto K, & Shaw JM (2005). Mitochondrial morphology and dynamics in yeast and multicellular eukaryotes. Annual Review of Genetics, 39, 503–536.

Park SB, Seo MS, Kim HS, & Kang KS (2012). Isolation and characterization of canine amniotic membrane-derived multipotent stem cells. PLOS One, 7(9), e44693. [PubMed: 23024756]

Sen U, Mishra PK, Tyagi N, & Tyagi SC (2010). Homocysteine to hydrogen sulfide or hypertension. Cell Biochemistry and Biophysics, 57(2–3), 49–58. [PubMed: 20387006]

Sharma DR, Sunkaria A, Wani WY, Sharma RK, Kandimalla RJ, Bal A, & Gill KD (2013). Aluminium induced oxidative stress results in decreased mitochondrial biogenesis via modulation of PGC-1alpha expression. Toxicology and Applied Pharmacology, 273(2), 365–380. [PubMed: 24084166]

Shum LC, White NS, Nadtochiy SM, Bentley KL, Brookes PS, Jonason JH, & Eliseev RA (2016). Cyclophilin D knock-out mice show enhanced resistance to osteoporosis and to metabolic changes observed in aging bone. PLOS One, 11(5), e0155709. [PubMed: 27183225]

Skovierova H, Vidomanova E, Mahmood S, Sopkova J, Drgova A, Cervenova T, … Lehotsky J (2016). The molecular and cellular effect of homocysteine metabolism imbalance on human health. International Journal of Molecular Sciences, 17(10), 1733.

Tyagi N, Ovechkin AV, Lominadze D, Moshal KS, & Tyagi SC (2006). Mitochondrial mechanism of microvascular endothelial cells apoptosis in hyperhomocysteinemia. Journal of Cellular Biochemistry, 98(5), 1150–1162. [PubMed: 16514665]

Vacek JC, Behera J, George AK, Kamat PK, Kalani A, & Tyagi N (2018). Tetrahydrocurcumin ameliorates homocysteine-mediated mitochondrial remodeling in brain endothelial cells. Journal of Cellular Physiology, 233(4), 3080–3092. [PubMed: 28833102]

Xi H, Zhang Y, Xu Y, Yang WY, Jiang X, Sha X, … Wang H (2016). Caspase-1 inflammasome activation mediates homocysteine-induced Pyrop-apoptosis in endothelial cells. Circulation Research, 118(10), 1525–1539. [PubMed: 27006445]

Xu ZS, Wang XY, Xiao DM, Hu LF, Lu M, Wu ZY, & Bian JS (2011). Hydrogen sulfide protects MC3T3-E1 osteoblastic cells against H2O2-induced oxidative damage-implications for the treatment of osteoporosis. Free Radical Biology and Medicine, 50(10), 1314–1323. [PubMed: 21354302]

Yang M, Huang Y, Chen J, Chen YL, Ma JJ, & Shi PH (2014). Activation of AMPK participates hydrogen sulfide-induced cyto-protective effect against dexamethasone in osteoblastic MC3T3-E1 cells. Biochemical and Biophysical Research Communications, 454(1), 42–47. [PubMed: 25445596]

Zhai Y, Li Y, Wang Y, Cui J, Feng K, Kong X, & Chen L (2017). Psoralidin, a prenylated coumestan, as a novel anti-osteoporosis candidate to enhance bone formation of osteoblasts and decrease bone resorption of osteoclasts. European Journal of Pharmacology, 801, 62–71. [PubMed: 28283388]

Zhai Y, Tyagi SC, & Tyagi N (2017). Cross-talk of MicroRNA and hydrogen sulfide: A novel therapeutic approach for bone diseases. Biomedicine & Pharmacotherapy, 92, 1073–1084. [PubMed: 28618652]

Zhai YK, Pan YL, Niu YB, Li CR, Wu XL, Fan WT, … Xian CJ (2014). The importance of the prenyl group in the activities of osthole in enhancing bone formation and inhibiting bone resorption in vitro. International Journal of Endocrinology, 2014, 921954. [PubMed: 25147567]

Zhang Y, He Y, Zong Y, Guo J, Sun L, Ma Y, … Gui L (2015). 17beta-estradiol attenuates homocysteine-induced oxidative stress and inflammatory response as well as MAPKs cascade via activating PI3-K/Akt signal transduction pathway in Raw 264.7 cells. Acta Biochimica et Biophysica Sinica, 47(2), 65–72. [PubMed: 25605419]

Zhu Y, Shen J, Cheng Q, Fan Y, & Lin W (2016). Plasma homocysteine level is a risk factor for osteoporotic fractures in elderly patients. Clinical Interventions in Aging, 11, 1117–1121. [PubMed: 27574411]

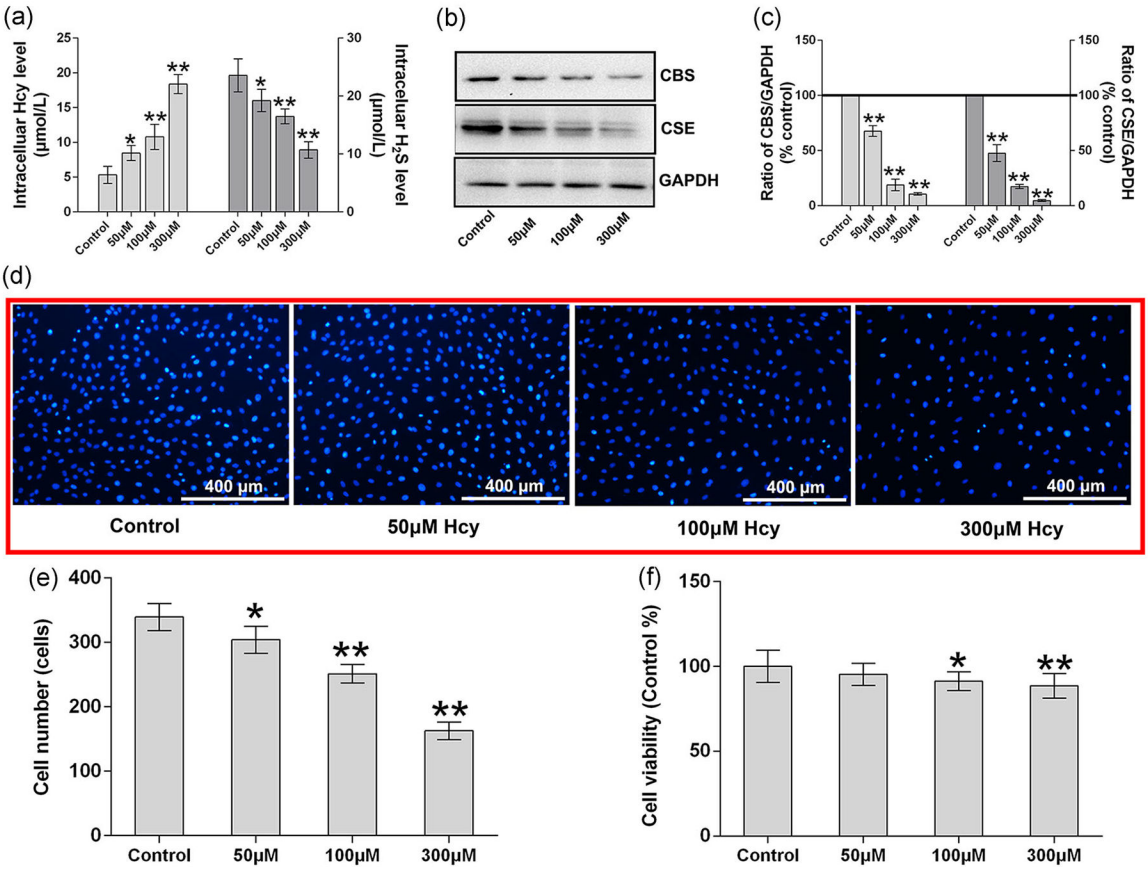

FIGURE 1.

Effect of Hcy effects on the H_2S metabolism and cell viability. (a) Intracellular level of Hcy and H_2S after supplemented with different dose of Hcy. (b, c) Western blot analysis of CBS and CSE expression. Quantitation of CBS and CSE by Image-Pro Plus 6.0 and displayed as relative optical density units after being standardized against GAPDH; (d) Hoechst 33342 staining of MC3T3-E1 cells; (e) quantitation of Hoechst 33342 staining and shown cell numbers; (f) cell viability analysis by MTT method. Values are means ± *SD*, $n = 6$, $^{*}p < 0.05$, $^{**}p < 0.01$ versus control. CBS: cystathionine β-synthase; CSE: cystathionine γ-lyase; GAPDH: glyceraldehyde 3-phosphate dehydrogenase; Hcy: homocysteine; H_2S: hydrogen sulfide; MTT: thiazolyl blue tetrazolium bromide

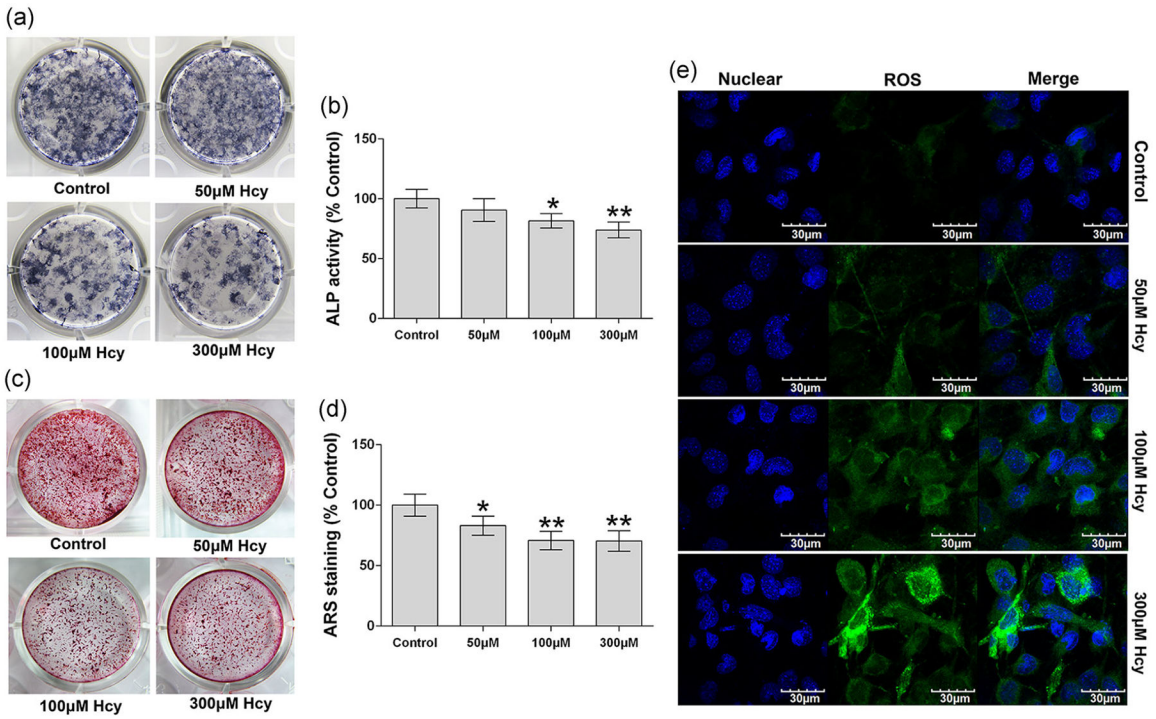

FIGURE 2.

Effects of Hcy on the osteoblast mineralization and total ROS production. (a) Colonies formation unit of ALP (CFU-ALP) in MC3T3-E1 cells. (b) ALP activity analysis. (c) Alizarin Red-S staining shown calcified nodules formation. (d) Quantitative analyses of calcified nodules. (e) Confocal imaging of DCFDA fluorescence staining shown total ROS production in MC3T3-E1 cell lines. Values are means ± *SD*, $n = 6$, $*p < 0.05$, $**p < 0.01$ versus control. ALP: alkaline phosphatase; DCFDA: 2′,7′-dichlorodihydrofluorescein diacetate; Hcy: homocysteine; ROS: reactive oxygen species

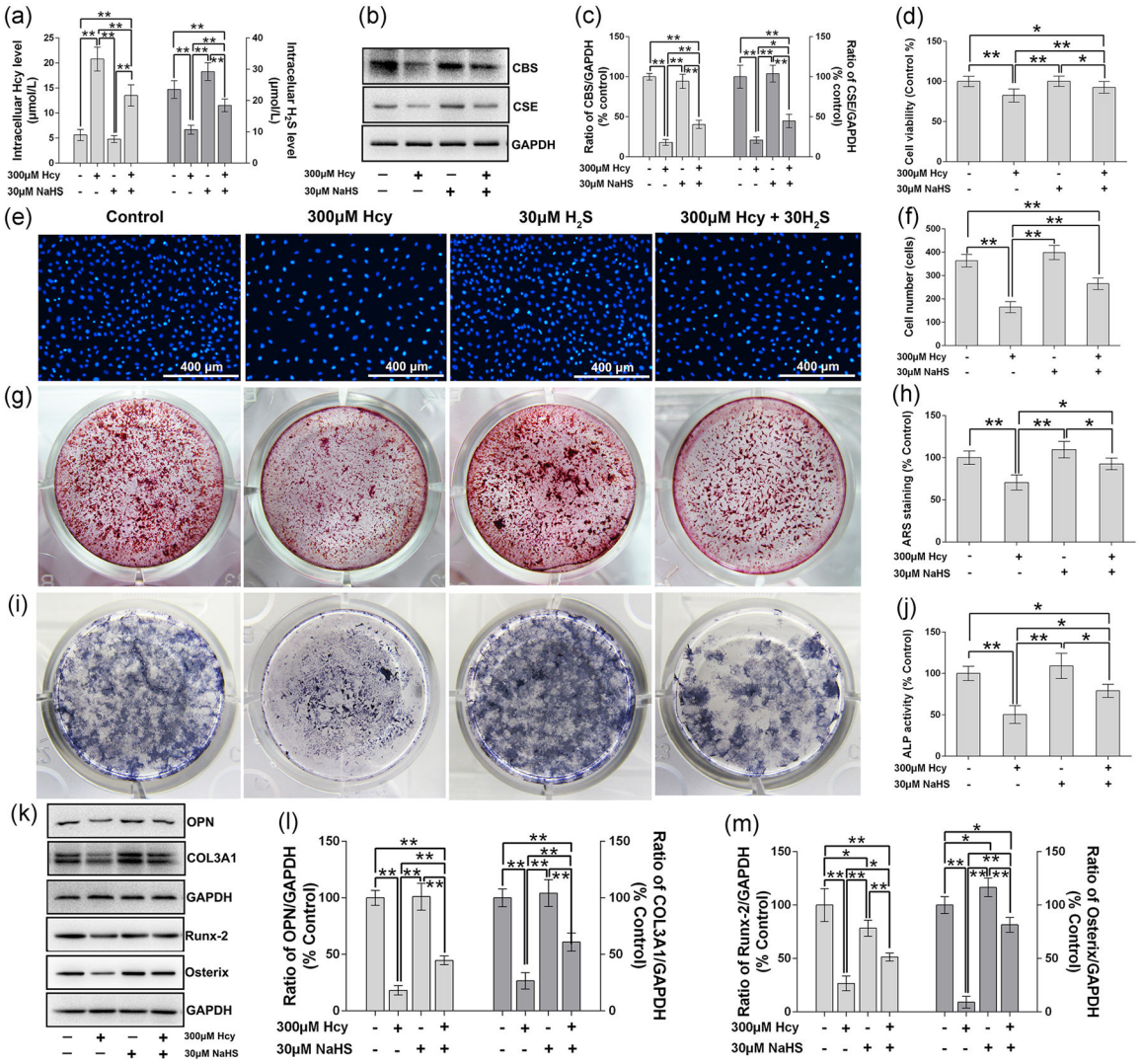

FIGURE 3.

Effect of NaHS on Hcy-induced toxic effects on cell viability and osteogenic differentiation of MC3T3-E1 cells. (a) Intracellular level of Hcy and H_2S. (b) Western blot results of CBS and CSE. (c) Quantitative analyses of CBS and CSE. (d) Cell viability analysis by MTT method. (e) Hoechst 33342 staining shown cell viability. (f) Cell number analysis based on the Hoechst 33342 staining. (g) Alizarin red-S staining to show calcified nodules formation. (h) Quantative analysis of Alizarin red S. (i) Colonies formation unit of ALP (CFU-ALP) staining. (j) ALP activity assay. (k) Western blot analysis of OPN, COL3A1, Runx-2 and Osterix protein expression. (l) Quantitative analyses of OPN and COL3A1. (m) Quantitative analyses of Runx-2 and Osterix. Values are means ± *SD*, $n = 6$, $^*p < 0.05$, $^{**}p < 0.01$ between two compared group. ALP: alkaline phosphatase; CBS: cystathionine β-synthase; CSE: cystathionine γ-lyase; COL3A1: collagen type III α1 chain; GAPDH: glyceraldehyde 3-phosphate dehydrogenase; Hcy: homocysteine; H_2S: hydrogen sulfide; MTT: thiazolyl blue tetrazolium bromide; NaHS: sodium hydrogen sulfide; OPN: osteopontin; Runx-2: runt-related transcription factor 2

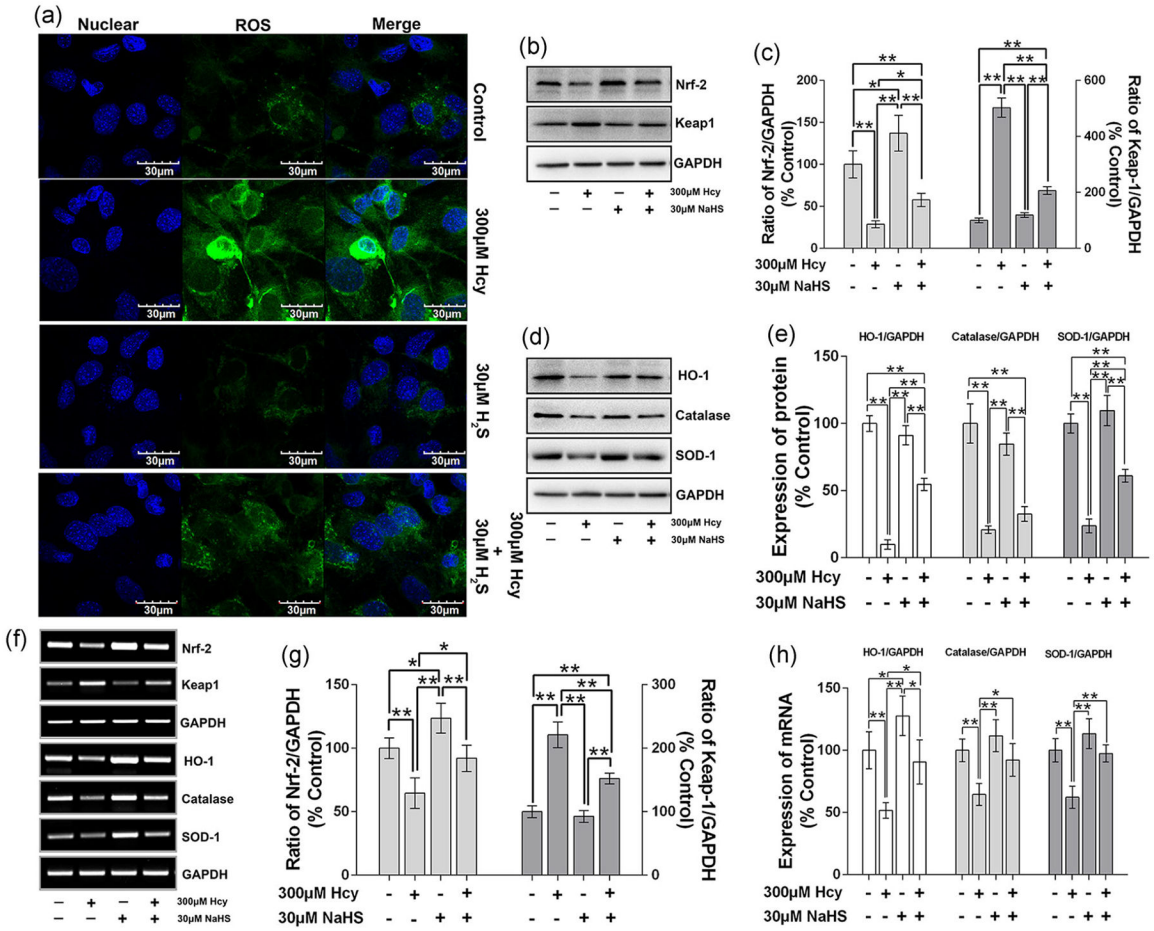

FIGURE 4.

NaHS attenuate Hcy-induced oxidative stress in MC3T3-E1 cells. (a) Representative images of total ROS production in cytoplasm by DCFDA staining. (b) Measurement of Nrf-2 and Keap-1 by western blot analysis. (c) Quantitative analyses of the expression of Nrf-2 and Keap-1. (d) Measurement of antioxidant factors (HO-1, catalase and SOD-1) by western blot expression. (e) Quantitative analyses of the expression of HO-1, catalase and SOD-1. (f) mRNA expression of related antioxidant factors using RT-PCR. (g) Quantitative analyses of the mRNA expression of Nrf-2 and Keap-1. (h) Quantitative analyses of the mRNA expression of HO-1, catalase and SOD-1. Values are means ± *SD*, $n = 6$, $^{*}p < 0.05$, $^{**}p < 0.01$ between two compared group. DCFDA: 2′,7′-dichlorodihydrofluorescein diacetate; Hcy: homocysteine; HO-1: heme oxygenase-1; Keap-1: kelch like ECH associated protein 1; mRNA: messenger RNA; NaHS: sodium hydrogen sulfide; Nrf-2: NF-E2-related factor 2; ROS: reactive oxygen species; RT-PCR: reverse transcription polymerase chain reaction; SOD-1: superoxide dismutase 1

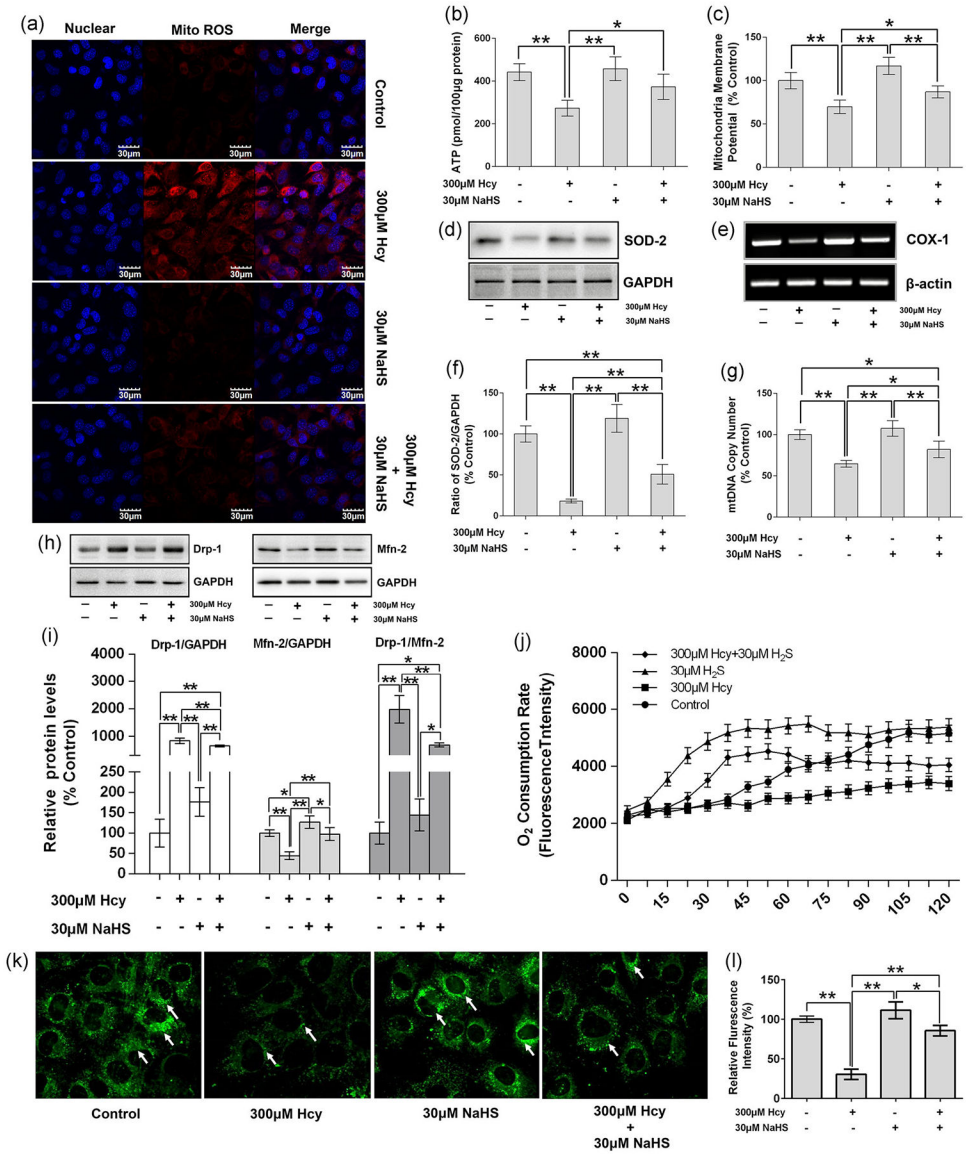

FIGURE 5.

NaHS attenuate Hcy-induced ROS generation in mitochondria and its dysfunction. (a) Representative images of ROS generation in mitochondria by Mito-Sox Red staining. (b) Measurement of ATP production. (c) MMP)analysis by JC-1 intake method. (d) Measurement of SOD-2 expression by western blot analysis. (e) Measurement of COX-1 by RT-PCR. (f) Quantitative analyses of the expression of SOD-2. (g) Quantitative analyses of the mtDNA copy number. (h) Measurement of the expression Drp-1 and Mfn-2 which represent the fission and fusion separately. (i) Quantitative analyses of the expression of Drp-1, Mfn-2, and ratio of Drp-1 and Mfn-2, results were normalized with control. (j) Measurement of the oxygen consumption rate. (k) Mitotracker green staining to show mitochondria. (l) Quantitative analysis of fluorescence intensity in mitotracker green staining. Values are means ± *SD*, $n = 6$, $^{*}p < 0.05$, $^{**}p < 0.01$ between two compared group. ATP: adenosine triphosphate; COX-1: cyclooxygenase 1; Drp-1: dynamin-related protein 1;

GAPDH: glyceraldehyde 3-phosphate dehydrogenase; Hcy: homocysteine; Mfn-2: mitofusin-2; MMP: mitochondria membrane potential; mtDNA: mitochondrial DNA; NaHS: sodium hydrogen sulfide; ROS: reactive oxygen species; RT-PCR: reverse transcription polymerase chain reaction; SOD-2: superoxide dismutase 2

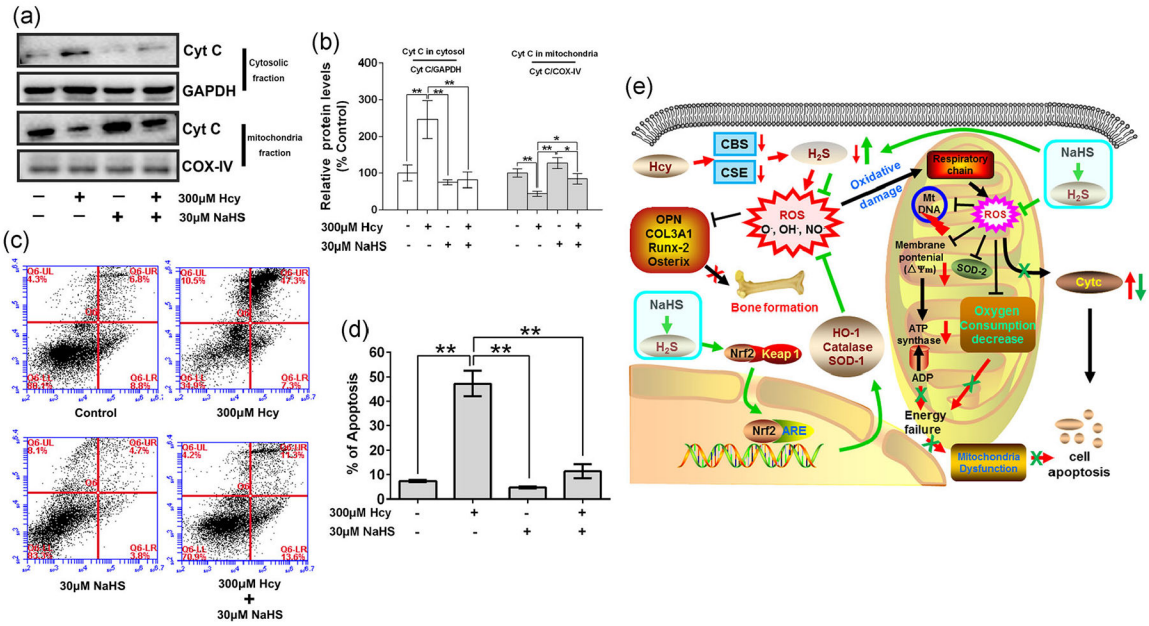

FIGURE 6.

NaHS decrease Hcy-mediated osteoblast apoptosis. (a) Expression of Cyt C in cytosolic fraction and mitochondria fraction which indicated the releasing of Cyt C during cell apoptosis. (b) Quantitation by Image-Pro Plus 6.0 and displayed as relative optical density units after being standardized against housekeeping gene bands, results were normalized with control group. (c) Annexin V/PI staining and flow cytometry to show cell apoptosis. (d) Quantification of flow cytometry to show the ratio of cell apoptosis. (e) Schematic of proposed hypothetical mechanism of NaHS mediated recovery of osteoblast function via mitochondrial biogenesis in Hcy-treated condition. Values are means ± *SD*, $n = 3$, $^{*}p < 0.05$, $^{**}p < 0.01$ between two compared group. Cyt C: cytochrome *c*; Hcy: homocysteine; NaHS: sodium hydrogen sulfide; PI: propidium iodide

TABLE 1

Primer sequences used for RT-PCR

Genes	Primer sequence
Nrf-2	Forward 5′-CAGTGCTCCTATGCGTGAA-3′
	Reverse 5′-GCGGCTTGAATGTTTGTC-3′
Keap-1	Forward 5′-GATCGGCTGCACTGAACTG-3′
	Reverse 5′-GGACTCGCAGCGTACGTT-3′
HO-1	Forward 5′-GACAGAAGAGGCTAAGACCGC-3′
	Reverse 5′-TGGAGGAGCGGTGTCTGG-3′
Catalase	Forward 5′-GCGGATTCCTGAGAGAGTGGTAC-3′
	Reverse 5′-GCCTGACTCTCCAGCGACTGTGGAG-3′
SOD-1	Forward 5′-CCAGTGCAGGACCTCATTTT-3′
	Reverse 5′-CACCTTTGCCCAAGTCATCT-3′
GAPDH	Forward 5′-ACCACAGTCCATGCCATCAC-3′
	Reverse 5′-TCCACCACCCTG TTGCTGTA-3′

Note. GAPDH: glyceraldehyde 3-phosphate dehydrogenase; HO-1: heme oxygenase-1; Keap-1: kelch like ECH associated protein 1; Nrf-2: NF-E2-related factor 2; RT-PCR: reverse transcription polymerase chain reaction; SOD-1: superoxide dismutase 1.